1

Solution of Singular Problems Using *h-p* Clouds

J. Tinsley Oden[1] and C. Armando Duarte[2]

Texas Institute for Computational and Applied Mathematics
The University of Texas at Austin
Taylor Hall 2.400
Austin, Texas, 78712, U.S.A.

[1]Professor, Director, TICAM. e-mail: oden@ticam.utexas.edu
[2]Research Assistant, TICAM. e-mail: armando@ticam.utexas.edu

1.1 INTRODUCTION

The *h-p* cloud technique [DO, DO95a] is a generalization of a family of so-called meshless methods (see, e.g., [BKOF96, LCJ+, Dua95] for an overview) proposed in recent months that provide both h and p (spectral) type approximations of boundary-value problems while freeing the analyst from traditional difficulties due to mesh connectivities. In these methods, the bounded domain of the solution of an elliptic boundary-value problem is covered by the union of a collection of open sets (the *clouds*) over which spectral-type approximation can be constructed. The mathematical foundation of these techniques applied to linear elliptic problems is discussed in [DO]. A-posteriori estimates and adaptive *h-p* clouds are developed in [DO95a].

In the present investigation, the generalization of *h-p* clouds to problems with singularities is presented. The theory of *h-p* clouds is reviewed following this introduction and adaptive *h-p* cloud techniques are outlined as well. Then the application of *h-p* clouds to problems with singularities is developed, particular attention being given to the calculation of stress intensity factors in linear fracture mechanics. A new scheme is presented for computing very accurate approximations of stress intensity factors. Several numerical examples are presented to support the theoretical developments.

1.2 *H-P* CLOUD APPROXIMATIONS

The fundamental idea in the *h-p* cloud method is to use a partition of unity to construct a hierarchy of functions that can represent polynomials of any degree. This family of functions, called $\mathcal{F}_N^p$, has many interesting properties like compact support and the ability to reproduce, through linear combinations, polynomials of any degree. In addition, the functions $\mathcal{F}_N^p$ can be built with any degree of regularity. Another remarkable feature of the functions $\mathcal{F}_N^p$ is that there is no need to partition the domain into smaller subdomains, e.g., finite elements, to construct these functions—all that is required is an arbitrarily placed set of nodes in the domain Ω. The construction of the functions $\mathcal{F}_N^p$, also known as *h-p* cloud functions, is described in the next section.

1.2.1 CONSTRUCTION OF A PARTITION OF UNITY

Let Ω be an open bounded domain in $\mathbb{R}^n$, $n = 1, 2$ or 3 and $\boldsymbol{Q}_N$ denote an arbitrarily chosen set of N points $\boldsymbol{x}_\alpha \in \bar{\Omega}$ referred to as *nodes*:

$$\boldsymbol{Q}_N = \{\boldsymbol{x}_1, \boldsymbol{x}_2, \ldots, \boldsymbol{x}_N\},\ \boldsymbol{x}_\alpha \in \bar{\Omega}$$

Let $\mathcal{T}_N := \{\omega_\alpha\}_{\alpha=1}^N$ denote a finite open covering of Ω consisting of N *clouds* ω_α with centers at $\boldsymbol{x}_\alpha$, $\alpha = 1, \ldots, N$ and having the following property

$$\bar{\Omega} \subset \bigcup_{\alpha=1}^{N} \bar{\omega}_\alpha \tag{1.1}$$

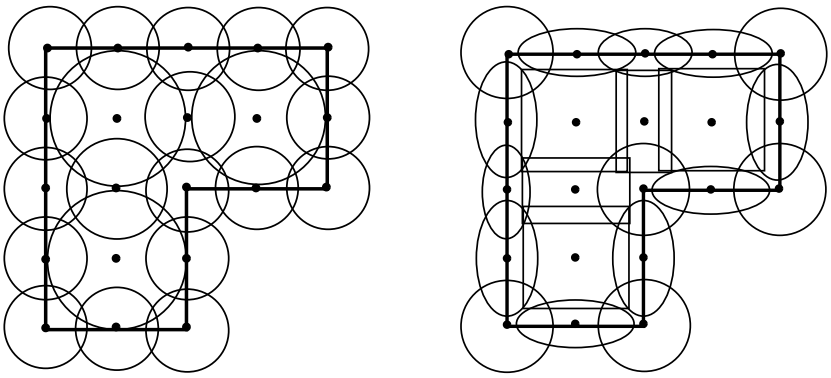

(a) Open covering build using circles.

(b) Open covering build using circles, ellipses and rectangles.

Figure 1 Examples of open coverings.

A cloud ω_α can be almost anything. In two dimensions, for example, it can be a rectangle, an ellipse or a circle. Figure 1 shows examples of valid open coverings and

associated clouds. In this paper we shall restrict ourselves to the case where a cloud ω_α is defined by

$$\omega_\alpha := \{\boldsymbol{y} \in \mathbb{R}^n |\ \|\boldsymbol{x}_\alpha - \boldsymbol{y}\|_{\mathbb{R}^n} < h_\alpha\} \tag{1.2}$$

This corresponds to the case shown in Fig. 1(a).

A class of functions $\mathcal{S}_N := \{\varphi_\alpha\}_{\alpha=1}^N$ is called a *partition of unity* subordinated to the open covering $\mathcal{T}_N$ if it possesses the following properties [OR76]:

1) $\varphi_\alpha \in C_0^\infty(\omega_\alpha), \qquad 1 \le \alpha \le N$

2) $\sum_{\alpha=1}^N \varphi_\alpha(\boldsymbol{x}) = 1, \qquad \forall\, \boldsymbol{x} \in \Omega$

Note that $\varphi_\alpha(\boldsymbol{x})$ may be negative.

There is no unique way to build functions φ_α satisfying the above requirements. Each approach has its own merits and embedded costs. The choice of a particular partition of unity should be based on

- the class of problems to be solved, e.g. linear or non-linear problems,
- the complexity of the geometry of the domain,
- the regularity required from the approximation, e.g. C^0, C^1, or higher,
- the importance of the meshless character of the approximation, etc.

The following algorithm is currently used the *h-p* cloud method to build partitions of unity.

Let $\mathcal{W}_\alpha : \mathbb{R}^n \to \mathbb{R}$ denote a *weighting function* with compact support ω_α that belongs to the space $C_0^s(\omega_\alpha)$, $s \ge 0$ and suppose that

$$\mathcal{W}_\alpha(\boldsymbol{x}) \ge 0 \qquad \forall\, \boldsymbol{x}\ \in \Omega$$

In the case of the clouds defined in (1.2), the weighting functions $\mathcal{W}_\alpha$ can be implemented with any degree of regularity using "ridge" functions. More specifically, the weighting functions $\mathcal{W}_\alpha$ can be implemented through the composition

$$\mathcal{W}_\alpha(\boldsymbol{x}) := g(r_\alpha)$$

where g is, e.g., a B-spline with compact support $[-1, 1]$ and r_α is the functional

$$r_\alpha := \frac{\|\boldsymbol{x} - \boldsymbol{x}_\alpha\|_{\mathbb{R}^n}}{h_\alpha}$$

In the computations presented in Section 1.3, g is a quartic $C^3(\Omega)$ B-spline. Details on the construction of the B-splines can be found in, e.g., [deB78].

The partition of unity functions φ_α can then be defined by

$$\varphi_\alpha(\boldsymbol{x}) = \frac{\mathcal{W}_\alpha(\boldsymbol{x})}{\sum_\beta \mathcal{W}_\beta(\boldsymbol{x})} \tag{1.3}$$

which are known as Shepard functions [She68]. The main advantages of this particular partition of unity are

- low computational cost and simplicity of computation,
- it is meshless—there is no need to partition the domain to build this partition of unity,
- it can easily be implemented in any dimension,
- it can be constructed with any degree of regularity
- it allows easy implementation of h adaptivity, as is demonstrated in Section 1.3.1.

1.2.2 THE FAMILY $\mathcal{F}_N^p$

The construction of the *h-p* cloud functions is very straightforward after a partition of unity is derived, such as the one described above, for the domain Ω.

Let $\widehat{\mathcal{L}}_p := \left\{\widehat{L}_i\right\}_{i\in\mathcal{I}}$, denote a set of *basis functions* $\widehat{L}_i$ defined on the unit cloud

$$\widehat{\omega} := \{\boldsymbol{\xi} \in \mathbb{R}^n |\ \|\boldsymbol{\xi}\|_{\mathbb{R}^n} < 1\}$$

satisfying

$$\begin{aligned} \widehat{L}_1(\boldsymbol{\xi}) &\equiv 1 \\ \mathcal{P}_p(\widehat{\omega}) &\subset \text{span}(\widehat{\mathcal{L}}_p) \end{aligned} \tag{1.4}$$

In the above, $\mathcal{I}$ denotes an index set and $\mathcal{P}_p$ denotes the space of polynomials of degree less or equal to p.

The family of functions $\mathcal{F}_N^p$ is defined by

$$\mathcal{F}_N^p := \left\{\varphi_\alpha(\boldsymbol{x})\left(\widehat{L}_i \circ \mathbf{F}_\alpha^{-1}(\boldsymbol{x})\right) \mid \alpha = 1,\ldots,N;\ i \in \mathcal{I}\right\} \tag{1.5}$$

where N is the number of nodes in the domain and

$$\mathbf{F}_\alpha^{-1} : \omega_\alpha \to \widehat{\omega} \tag{1.6}$$

$$\mathbf{F}_\alpha^{-1}(\boldsymbol{x}) := \frac{\boldsymbol{x} - \boldsymbol{x}_\alpha}{h_\alpha}$$

According to the above definition, $\mathcal{F}_N^p$ is constructed by multiplying each partition of unity function $\varphi_\alpha \in \mathcal{S}_N$ by the elements from the set $\widehat{\mathcal{L}}_p$. One element from the space of *h-p* cloud functions can therefore be written as

$$u^{hp}(\boldsymbol{x}) = \sum_{\alpha=1}^{N}\sum_{i\in\mathcal{I}}\left[a_{\alpha i}\varphi_\alpha(\boldsymbol{x})(\widehat{L}_i \circ \mathbf{F}_\alpha^{-1}(\boldsymbol{x}))\right]$$

The following theorems are proved in [DO].

Theorem 1 *Let* $\mathcal{L}_p := \{L_i\}_{i\in\mathcal{I}}$ *and* L_i *be the same functions* $\widehat{L}_i$ *but defined on* Ω. *Then* $\mathcal{L}_p \subset span\{\mathcal{F}_N^p\}$,

Therefore the elements from the set $\mathcal{L}_p$ can be recovered through linear combinations of the *h-p* clouds functions. This is one of the most fundamental properties of the *h-p* cloud functions.

Theorem 2 *Let* $\widehat{L}_i,\ i \in \mathcal{I}$, *be the basis functions from the set* $\widehat{\mathcal{L}}_p$ *and* $\mathcal{W}_\alpha,\ \alpha = 1,\ldots,N$ *be the weighting functions used to construct the partition of unity functions* φ_α *defined in (1.3). Suppose that* $\widehat{L}_i,\ i \in \mathcal{I} \in C^l(\widehat{\omega})$ *and* $\mathcal{W}_\alpha,\ \alpha = 1,\ldots,N \in C_0^q(\omega_\alpha)$. *Then the h-p cloud functions* $\mathcal{F}_N^p$ *defined in (1.5) belong to the space* $C_0^{min(l,q)}(\Omega)$.

Figure 2(a) shows the partition of unity function φ_α associated with a node $\boldsymbol{x}_\alpha$ at the origin. A uniform 5×5 node arrangement and quartic splines are used to build it. Figure 2(b) shows the function $xy\varphi_\alpha$ from the families $\mathcal{F}_{N=25}^{p\geq 2}$.

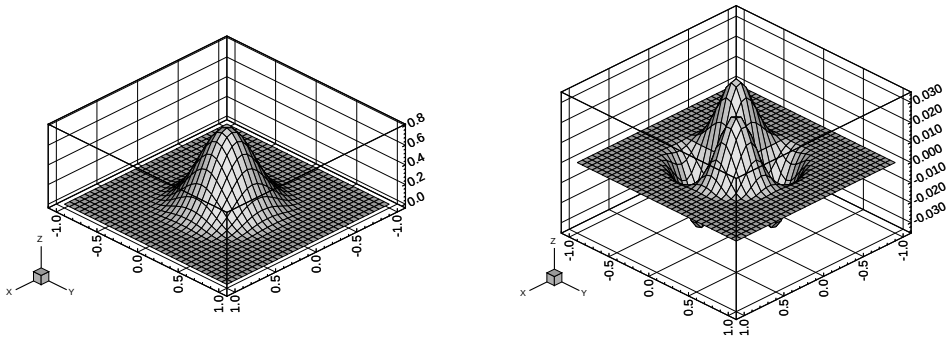

(a) 2-D partition of unity function φ_α.

(b) 2-D h-p cloud function $xy\varphi_\alpha$ from the families $\mathcal{F}_{N=25}^{p\geq 2}$.

Figure 2 2-D h-p cloud functions.

Remark 1 *There are many cases in which there is some knowledge about the function being approximated and the requirement that* $\mathcal{P}_p(\widehat{\omega}) \subset span(\widehat{\mathcal{L}}_p)$ *can be weakened without deteriorating the approximating properties of the set* $\widehat{\mathcal{L}}_p$ *[BM95]. There are also situations in which the inclusion in the set* $\widehat{\mathcal{L}}_p$ *of specially tailored functions to model, e.g., boundary layers, shocks, singularities, etc., can be very advantageous. This is the case in the stress analysis of cracks where the quantities of interest are the stress intensity factors. This case is discussed in detail in Section 1.3.2.*

An a-priori estimate

In this section we summarize some results presented in [DO].

Let $\boldsymbol{X}_\alpha^{hp}$ be the restriction to $(\Omega \cap \omega_\alpha)$ of the elements from the two parameters (p and $h(N)$) family of spaces

$$\widetilde{\boldsymbol{X}}_\alpha^{hp}(\omega_\alpha) := span\left\{\widehat{L}_i \circ \mathbf{F}_\alpha^{-1}\right\}_{i\in\mathcal{I}}$$

where the mapping $\mathbf{F}_\alpha^{-1}$ is defined in (1.6) and $\widehat{L}_i \in \widehat{\mathcal{L}}_p$.

Theorem 3 *Let* $u \in H^{r+1}(\Omega)$, $r \geq 0$. *Suppose that the following hold for all local spaces* $\boldsymbol{X}_\alpha^{hp}$

$$\mathcal{P}_r(\Omega \cap \omega_\alpha) \subset \boldsymbol{X}_\alpha^{hp} \subset H^1(\Omega \cap \omega_\alpha)$$

Then for fixed h *and* p *there is* $u_{hp} \in \boldsymbol{X}^{hp} := span\{\mathcal{F}_N^p\}$ *such that*

$$\|u - u_{hp}\|_{L^2(\Omega)} \leq C_1 h^{r+1} \|u\|_{H^{r+1}(\Omega)}, \tag{1.7}$$

$$\|u - u_{hp}\|_{H^1(\Omega)} \leq C_2 h^{r} \|u\|_{H^{r+1}(\Omega)} \tag{1.8}$$

where the constants C_1 and C_2 do not depend on h or u but depend on p, and $h = \max_{\alpha=1,\ldots,N(h)} h_\alpha$.

An a-posteriori error estimate

Let $\Omega \subset \mathbb{R}^2$ be a bounded domain with Lipschitz boundary $\partial\Omega$. Consider the model elliptic boundary-value problem of finding the solution u of

$$-\Delta u + cu = f \qquad in\ \Omega$$

subject to the boundary conditions

$$\begin{aligned} \frac{\partial u}{\partial n} &= g \qquad on\ \Gamma_N \\ u &= 0 \qquad on\ \Gamma_D \end{aligned}$$

The variational form of this problem is to find $u \in V_D$ such that

$$B(u,v) = L(v) \qquad \forall\ v \in V_D$$

where V_D is the space

$$V_D = \{v \in H^1(\Omega) : v = 0\ on\ \Gamma_D\}$$

and where

$$\begin{aligned} B(u,v) &= \int_\Omega (\nabla u \cdot \nabla v + cuv)\, d\boldsymbol{x} \\ L(v) &= \int_\Omega fv\, d\boldsymbol{x} + \int_{\Gamma_N} gv\, d\boldsymbol{x} \end{aligned}$$

Suppose that $\boldsymbol{X}^{hp} \subset V_D$ is a subspace built using *h-p* clouds. Then the *h-p* cloud-Galerkin approximation of this problem is to find $u_{hp} \in \boldsymbol{X}^{hp}$ such that

$$B(u_{hp}, v_{hp}) = L(v_{hp}) \qquad \forall\ v_{hp} \in \boldsymbol{X}^{hp}$$

The following is proved in [DO95a].

Theorem 4 *Suppose that $\boldsymbol{X}^{hp} \subset (C^2(\Omega) \cap V_D)$. Let r denote the interior residual*

$$r = f + \Delta u_{hp} - cu_{hp} \qquad in\ \Omega$$

and R denote the boundary residual

$$R = g - \frac{\partial u_{hp}}{\partial n} \qquad on\ \Gamma_N$$

Then the energy norm of the discretization error $e = u - u_{hp}$ satisfies

$$\|e\|_{E,\Omega} \leq \rho^{1/2} \bar{C} \left(\sum_\alpha \eta_\alpha^2 \right)^{1/2}$$

where the contributions η_α from the clouds ω_α are error indicators and are given by

$$\eta_\alpha^2 = \frac{h_\alpha^2}{p_\alpha^2} \|r\|^2_{L^2(\omega_\alpha \cap \Omega)} + \frac{h_\alpha}{p_\alpha} \|R\|^2_{L^2(\partial(\omega_\alpha \cap \Omega) \cap \Gamma_N)} \tag{1.9}$$

and $\rho \in \mathbb{N}$ satisfies

$$card\{\alpha | \boldsymbol{x} \in \omega_\alpha\} \leq \rho \qquad \forall\ \boldsymbol{x} \in \Omega$$

The error indicators η_α are used in Section 1.3.1 to implement h, p and h-p adaptivity in the h-p cloud method.

1.3 NUMERICAL EXAMPLES

In this section, the techniques described in Section 1.2 are used to construct appropriate finite dimensional subspaces of functions used in the Galerkin method. The resulting approach is denoted as the *h-p cloud method*. Two problems are solved in this section using the h-p cloud method. The first problem demonstrates how h, p and h-p adaptivity can be implemented in the h-p cloud method and how the method can handle the presence of a singularity. The second problem deals with the stress analysis of cracks in linear elasticity and the computation of stress intensity factors. We explore the fact that the h-p cloud spaces are able include almost any kind of function and develop a novel and very efficient approach to extract stress intensity factors. It is demonstrated numerically that the computed stress intensity factors converge at the same rate as the error in energy and, therefore, at twice the rate of the error in the energy norm.

In all problems solved the following is adopted:

- The essential boundary conditions are imposed using the method of Lagrange multipliers.
- The domain integrations are performed using a background cell structure that exactly covers the domains. Nonetheless, there is no relationship between the background cell structures and the nodes $\boldsymbol{x}_\alpha$ used in the discretizations. It should be noted that the generation of a background cell structure is much easier than the generation of a traditional finite element mesh.
- The algorithm presented in [DO95a] is used to handle re-entrant corners.
- In all problems analyzed, the size of the supports of the h-p cloud functions are automatically set using the algorithm presented in [DO95b, DO].

1.3.1 POTENTIAL FLOW IN A L-SHAPED DOMAIN

In this section, a potential flow problem in a L-shaped domain is solved using the h-p cloud method. The problem statement is given below. The domain Ω and the boundary segments Γ_1 and Γ_2 are depicted in Fig. 3. The value of u is set to zero at $(1, 1)$ in order to make the solution unique. This simple boundary-value problem is used to demonstrate how h, p and h-p adaptivity can be implemented in the h-p cloud method without using the concept of a mesh and how adaptivity can be used in the h-p cloud method to handle the presence of singularities.

Find u such that

$$\begin{aligned} -\Delta u &= 0 \quad in\ \Omega \\ -\frac{\partial u}{\partial n} &= 5 \quad on\ \Gamma_1 \\ -\frac{\partial u}{\partial n} &= -5 \quad on\ \Gamma_2 \\ -\frac{\partial u}{\partial n} &= 0 \quad on\ \partial\Omega\backslash(\Gamma_1 \cup \Gamma_2) \end{aligned} \tag{1.10}$$

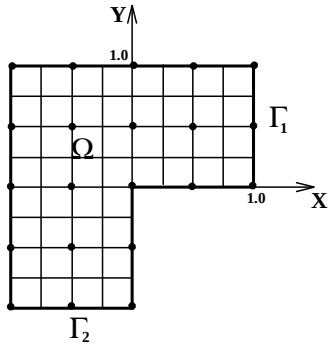

Figure 3 Boundary conditions, initial nodal arrangement and background cell structure used for quadrature.

For this problem, the set of functions $\widehat{\mathcal{L}}_p(\widehat{\omega})$ defined in (1.4) is composed of the following monomials:

$$\widehat{\mathcal{L}}_p(\widehat{\omega}) = \{\xi^i \eta^j | 0 \leq i + j \leq p\}$$

That is, the family of h-p cloud functions, $\mathcal{F}_N^p$, is constructed by multiplying the partition of unity functions φ_α, $\alpha = 1, \ldots, N$, by the smallest set of complete polynomials of degree less or equal to p.

The background cell structure used to perform the numerical quadrature is represented in Fig. 3. The nodal arrangement used in the first step of h, p and h-p adaptation is also shown in the figure.

h adaptivity

Theorem 3 demonstrates that the discretization error of the h-p cloud solution can be controlled by decreasing the radius h_α of the clouds. This, of course, has to be followed by the addition of more nodes to the discretization in order to guarantee that a valid covering for the domain still exists. It should be noted, however, that there is no constraint on how these nodes are placed in the domain—they can simply be inserted into the regions of interest. This strategy is denoted the h *version* of the h-p cloud method. This approach is demonstrated in the solution of problem (1.10). Details of the algorithm used in the h version of the h-p cloud method can be found [DO95a]. The nodal arrangement represented in Fig. 3 and clouds with polynomial degree $p = 1$ are used to obtain the first approximate solution. The error indicators given by (1.9) are then computed for each cloud ω_α. Clouds with errors above a preset value are selected to be refined while the polynomial order is kept fixed. The refinement of clouds involves the addition of news nodes around each of the refined clouds. The size of the supports ω_α are then automatically reset to take into account the new nodes added to the discretization (details of the algorithm can be found in [DO]). A new solution is then computed using the new discretization and the process is repeated until the quality of the solution is deemed acceptable.

Figure 4 shows the nodal arrangement and the covering obtained after seven steps of h adaptation. A high concentration of nodes near the corner at $(0, 0)$ is observed.

Figure 5 depicts the fluxes computed using the discretization of Fig. 4. The color associated with each arrow represents the computed potential u_h. The flux distribution indicates the presence of a singularity at the re-entrant corner at $(0,0)$.

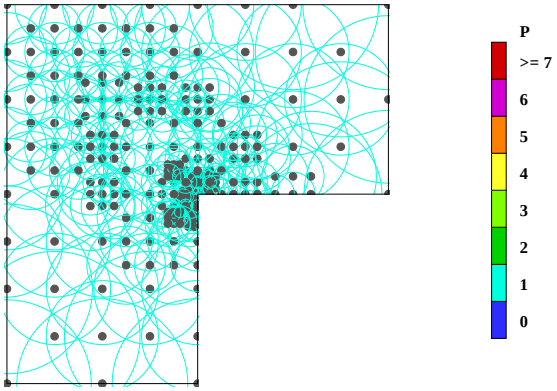

Figure 4 Discretization obtained using h adaptivity.

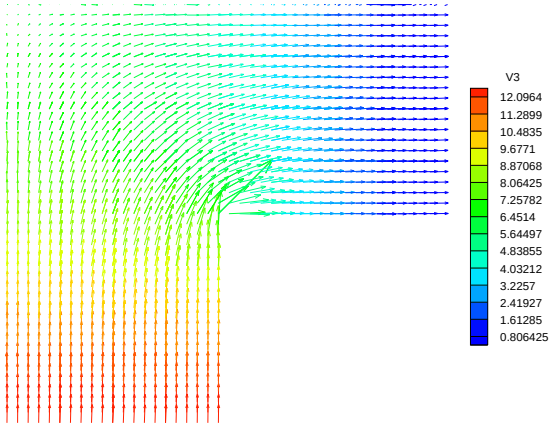

Figure 5 Flux distribution.

p adaptivity

In the p version of the h-p cloud method, the solution space is enriched by keeping fixed the size h_α of the clouds and increasing the polynomial order p associated with each cloud. It is noted that each cloud ω_α can have a different polynomial order associated with it, *independently* of the polynomial order associated with neighboring clouds.

Figure 6(a) shows the polynomial orders associated with each cloud after six steps of p adaptation. The polynomial orders assigned to each cloud is automatically chosen using the error indicators given by (1.9). The polynomial orders range from $p = 1$ to

$p = 7$. Figure 6(b) represents the potential u_p computed using the discretization of Fig. 6(a).

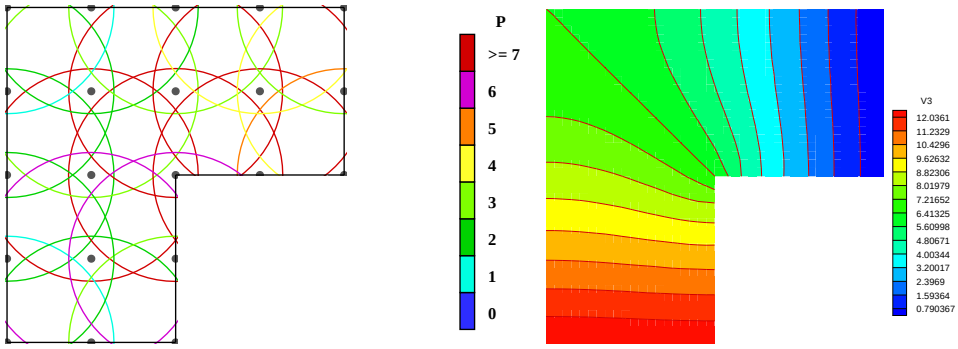

(a) Discretization obtained using p adaptivity.

(b) Solution obtained using p adaptivity.

Figure 6 Results from the p version of the h-p cloud method

h-p adaptivity

The h-p version of the h-p cloud method is implemented by combining the h and p algorithms described previously. Two or more steps of h adaptation are initially performed in order to isolate any singularity present in the solution. This is followed by a number of p steps until the estimated error is below a preset value. In the case of problem (1.10), two h steps are initially performed, starting from the nodal arrangement of Fig. 3. After that, the error is controlled through p enrichment of the clouds. The final discretization is presented in Fig. 7. Figure 8(a) shows the computed fluxes and potential. The three dimensional plot of Fig. 8(b) presents the computed flux in the y direction using the discretization of Fig. 7. The presence of a singularity at $(0, 0)$ is evident.

1.3.2 MODELING OF CORNER SINGULARITIES AND COMPUTATION OF STRESS INTENSITY FACTORS IN LINEAR FRACTURE MECHANICS

In this section, we demonstrate how corner singularities in plane elasticity problems can be efficiently modeled using the framework of h-p clouds. These singularities occur when the solution domain has corners, abrupt changes in boundary data or consists of two or more materials [OB95]. The h-p cloud results are compared with those of the p version of the finite element method. We also present a new approach for the extraction of the amplitude of the singular terms associated with corner singularities. The accuracy and simplicity of this novel approach is demonstrated numerically.

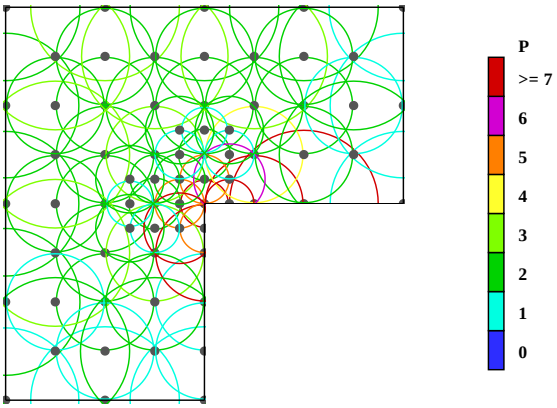

Figure 7 Discretization obtained using h-p adaptivity.

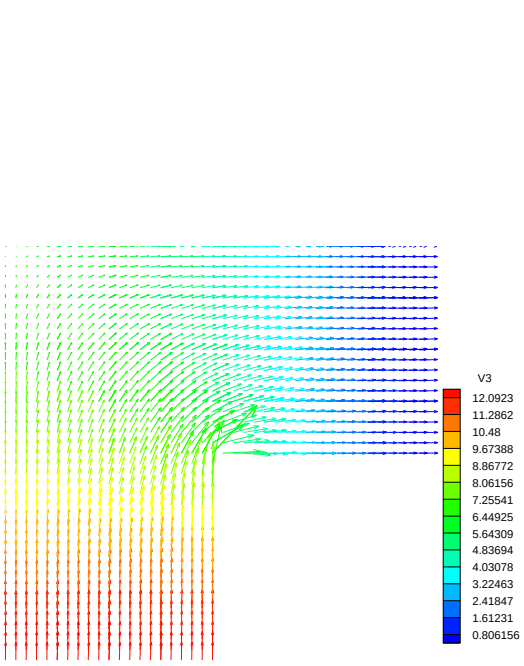

(a) Flux distribution.

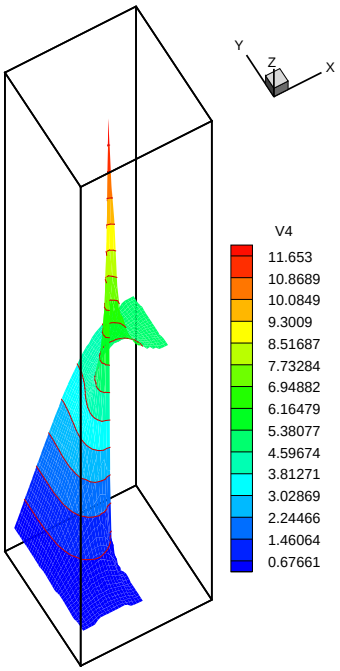

(b) Flux in the y direction obtained using h-p adaptivity.

Figure 8 Results obtained using h-p adaptivity.

Near crack tip expansion

In the neighborhood of a crack, assuming traction-free crack surfaces and in the absence of body forces, each component of the displacement vector $\boldsymbol{u} = \{u_x, u_y\}^T$ can be written as [SB91, SB88]

$$u_x(r,\theta) = \sum_{j=1}^{M} \left(A_j^{(1)} u_{xj}^{(1)}(r,\theta) + A_j^{(2)} u_{xj}^{(2)}(r,\theta) \right) + \tilde{u}_x(r,\theta) \tag{1.11}$$

$$u_y(r,\theta) = \sum_{j=1}^{M} \left(A_j^{(1)} u_{yj}^{(1)}(r,\theta) + A_j^{(2)} u_{yj}^{(2)}(r,\theta) \right) + \tilde{u}_y(r,\theta) \tag{1.12}$$

where (r,θ) are the polar coordinates associated with the crack tip (cf. Fig. 9), $\tilde{u}_x(r,\theta)$ and $\tilde{u}_y(r,\theta)$ are functions smoother than any term in the sum and the eigenfunctions are given by

$$\begin{aligned}
u_{xj}^{(1)}(r,\theta) &= \frac{r^{\lambda_j}}{2G} \left\{ [\kappa - Q_j^{(1)}(\lambda_j + 1)] \cos \lambda_j \theta - \lambda_j \cos(\lambda_j - 2)\theta \right\} \\
u_{xj}^{(2)}(r,\theta) &= \frac{r^{\lambda_j}}{2G} \left\{ [\kappa - Q_j^{(2)}(\lambda_j + 1)] \sin \lambda_j \theta - \lambda_j \sin(\lambda_j - 2)\theta \right\} \\
u_{yj}^{(1)}(r,\theta) &= \frac{r^{\lambda_j}}{2G} \left\{ [\kappa + Q_j^{(1)}(\lambda_j + 1)] \sin \lambda_j \theta + \lambda_j \sin(\lambda_j - 2)\theta \right\} \\
u_{yj}^{(2)}(r,\theta) &= -\frac{r^{\lambda_j}}{2G} \left\{ [\kappa + Q_j^{(2)}(\lambda_j + 1)] \cos \lambda_j \theta + \lambda_j \cos(\lambda_j - 2)\theta \right\}
\end{aligned}$$

where the eigenvalues λ_j are

$$\lambda_1 = \frac{1}{2}, \qquad \lambda_j = \frac{j+1}{2} \qquad j \geq 2$$

and

$$Q_j^{(1)} = \begin{cases} -1 & j = 3,5,7,\ldots \\ -\Lambda_j & j = 1,2,4,6,\ldots \end{cases} \qquad Q_j^{(2)} = \begin{cases} -1 & j = 1,2,4,6,\ldots \\ -\Lambda_j & j = 3,5,7,\ldots \end{cases}$$

where

$$\Lambda_j = \frac{\lambda_j - 1}{\lambda_j + 1}$$

and the material constant κ and G are

$$\kappa = \begin{cases} 3 - 4\nu & \text{plane strain} \\ \frac{3-\nu}{1+\nu} & \text{plane stress} \end{cases} \qquad G = \frac{E}{2(1+\nu)}$$

where E is the Young's modulus and ν is the Poisson's ratio.

The coefficients $A_1^{(1)}$ and $A_1^{(2)}$ in (1.11) and (1.12) are related to the Mode I and Mode II stress intensity factors of linear elasticity fracture mechanics, usually denoted by K_I and K_{II}, as follows:

$$A_1^{(1)} = \frac{K_I}{\sqrt{2\pi}} \qquad A_1^{(2)} = \frac{K_{II}}{\sqrt{2\pi}}$$

Enrichment of the h-p cloud spaces and extraction of stress intensity factors

Suppose that the eigenfunctions $u_{xj}^{(1)},\ u_{xj}^{(2)},\ u_{yj}^{(1)},\ u_{yj}^{(2)},\ j=1,\ldots,M$ are added to the set $\widehat{\mathcal{L}}_p$ defined in Section 1.2.2 giving

$$\widehat{\mathcal{L}}_p^* := \left\{\widehat{L}_i\right\}_{i\in\mathcal{I}} \cup \left\{u_{xj}^{(1)},\ u_{xj}^{(2)},\ u_{yj}^{(1)},\ u_{yj}^{(2)}\right\}_{j=1,\ldots,M} \tag{1.13}$$

Then, the enriched h-p cloud functions are defined as follows

$$\begin{aligned}\mathcal{F}_N^{p*} \quad := \quad & \left\{\ \varphi_\alpha(\boldsymbol{x})\left[\widehat{L}_i\circ\mathbf{F}_\alpha^{-1}(\boldsymbol{x})\right] \cup \varphi_\alpha(\boldsymbol{x})\left[\bar{u}_{xj}^{(1)}(\boldsymbol{x}),\bar{u}_{xj}^{(2)}(\boldsymbol{x}),\bar{u}_{yj}^{(1)}(\boldsymbol{x}),\bar{u}_{yj}^{(2)}(\boldsymbol{x})\right]\right. \\ & \left.\ |\ \alpha=1,\ldots,N;\ i\in\mathcal{I};\ j=1,\ldots,M\ \right\}\end{aligned} \tag{1.14}$$

where

$$\bar{u}_{xj}^{(1)}(\boldsymbol{x}) := u_{xj}^{(1)}\circ\mathbf{T}^{-1}(\boldsymbol{x})$$

and $\mathbf{T}^{-1}$ is the transformation from rectangular to polar coordinates. The other bar quantities are computed similarly and the transformation $\mathbf{F}^{-1}$ is defined in (1.6). Note that all elements from $\mathcal{F}_N^{p*}$ have compact support.

The h-p cloud approximation to the displacement field (1.11),(1.12) can be written as

$$\begin{aligned}u_x^{hp}(\boldsymbol{x}) \quad = \quad & \sum_{\alpha=1}^{N}\sum_{i\in\mathcal{I}}\left[a_x^{\alpha i}\varphi_\alpha(\boldsymbol{x})(\widehat{L}_i\circ\mathbf{F}_\alpha^{-1}(\boldsymbol{x}))\right] \\ & + \sum_{\alpha=1}^{N}\sum_{j=1}^{M}\left[b_{\alpha j}^{(1)}\varphi_\alpha(\boldsymbol{x})\,\bar{u}_{xj}^{(1)}(\boldsymbol{x}) + b_{\alpha j}^{(2)}\varphi_\alpha(\boldsymbol{x})\bar{u}_{xj}^{(2)}(\boldsymbol{x})\right] \\ u_y^{hp}(\boldsymbol{x}) \quad = \quad & \sum_{\alpha=1}^{N}\sum_{i\in\mathcal{I}}\left[a_y^{\alpha i}\varphi_\alpha(\boldsymbol{x})(\widehat{L}_i\circ\mathbf{F}_\alpha^{-1}(\boldsymbol{x}))\right] \\ & + \sum_{\alpha=1}^{N}\sum_{j=1}^{M}\left[b_{\alpha j}^{(1)}\varphi_\alpha(\boldsymbol{x})\,\bar{u}_{yj}^{(1)}(\boldsymbol{x}) + b_{\alpha j}^{(2)}\varphi_\alpha(\boldsymbol{x})\bar{u}_{yj}^{(2)}(\boldsymbol{x})\right]\end{aligned}$$

In the above expansion, for a fixed $\boldsymbol{x}\in\bar{\Omega}$, only a few terms are nonzero since all the functions have compact support. The expansion for, e.g., u_x^{hp} can be rewritten as

$$u_x^{hp}(\boldsymbol{x}) \quad = \quad \underbrace{\sum_{\alpha=1}^{N}\sum_{i\in\mathcal{I}}\left[a_x^{\alpha i}\varphi_\alpha(\boldsymbol{x})(\widehat{L}_i\circ\mathbf{F}_\alpha^{-1}(\boldsymbol{x}))\right]}_{\text{polynomial reproducing part}} + \underbrace{\sum_{j=1}^{M}[\bar{u}_{xj}^{(1)}(\boldsymbol{x})\overbrace{\sum_{\alpha=1}^{N}b_{\alpha j}^{(1)}\varphi_\alpha(\boldsymbol{x})}^{A_j^{(1)}}]}_{\text{singular part}}$$

$$+\underbrace{\sum_{j=1}^{M}[\bar{u}_{xj}^{(2)}(\boldsymbol{x})\overbrace{\sum_{\alpha=1}^{N}b_{\alpha j}^{(2)}\varphi_\alpha(\boldsymbol{x})}^{A_j^{(2)}}]}_{\text{singular part}} \tag{1.15}$$

Comparing (1.15) with (1.11) leads to the following conclusion: the term $\tilde{u}_x$ can be approximated very accurately by the polynomial part of u_x^{hp} since it is a smooth function. Therefore the difference between $\tilde{u}_x$ and the polynomial part of u_x^{hp} can be made as small as we want (possibly exponentially) by increasing the polynomial order associated with the clouds; consequently we must expect that

$$\sum_{\alpha=1}^{N} b_{\alpha j}^{(1)}\varphi_\alpha \overset{p\to\infty}{\longrightarrow} A_j^{(1)} \qquad \text{and} \qquad \sum_{\alpha=1}^{N} b_{\alpha j}^{(2)}\varphi_\alpha \overset{p\to\infty}{\longrightarrow} A_j^{(2)}$$

Therefore the amplitude of *any number* of generalized stress intensity factors can be obtained directly from the coefficient of the *h-p* cloud functions without any additional work. The first and second stress intensity factors from linear fracture mechanics are therefore given by

$$K_I = \sqrt{2\pi}A_1^{(1)} = \sqrt{2\pi}\sum_{\alpha=1}^{N} b_{\alpha 1}^{(1)}\varphi_\alpha$$

$$K_{II} = \sqrt{2\pi}A_1^{(2)} = \sqrt{2\pi}\sum_{\alpha=1}^{N} b_{\alpha 1}^{(2)}\varphi_\alpha$$

Remark 2 *The case of more complicated boundary conditions at the crack surfaces can be treated exactly as above [OB95]. In the case of anisotropic or nonhomogenous materials, the numerical approach proposed by [PB95] can be used to compute the eigenvalues and eigenfunctions of the asymptotic expansion near the crack tip. The approach described above can then be used without any modifications.*

Cracked panel

In this section, the edge-cracked panel shown in Fig. 9 is analyzed using the enriched *h-p* cloud spaces $\mathcal{F}_N^{p*}$ defined in (1.14). The *h-p* cloud results are compared with those presented by Szabo [Sza86] and Duarte and Barcellos [DdB91] for the p version of the finite element method using strongly graded meshes.

A state of plane-strain, Poisson's ratio of 0.3 and unity thickness are assumed. The tractions corresponding to the first symmetric term of the asymptotic expansion (1.11), (1.12) are applied on $\partial\Omega$. The two components of the displacement at $(0,0)$ and the vertical component at $(d,0)$ are set to zero to make the solution unique. The components of the stress tensor associated with the first term of the asymptotic expansion are given by [SB91]

$$\sigma_{ij}^{(1)} = \frac{K_I}{\sqrt{2\pi r}} f_{ij}^{(1)}(\theta) \tag{1.16}$$

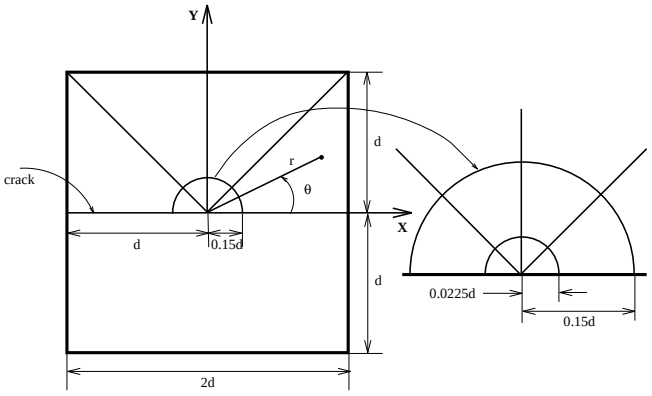

Figure 9 Cracked panel and geometric mesh with three layers of finite elements.

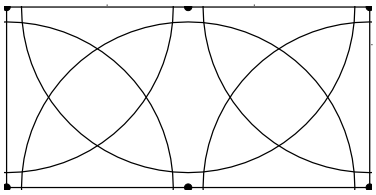

Figure 10 *h-p* cloud discretization for the cracked panel.

$$f_{11}^{(1)}(\theta) = \cos\left(\frac{\theta}{2}\right)\left[1-\sin\left(\frac{\theta}{2}\right)\sin\left(\frac{3\theta}{2}\right)\right] \tag{1.17}$$

$$f_{22}^{(1)}(\theta) = \cos\left(\frac{\theta}{2}\right)\left[1+\sin\left(\frac{\theta}{2}\right)\sin\left(\frac{3\theta}{2}\right)\right] \tag{1.18}$$

$$f_{12}^{(1)}(\theta) = \cos\left(\frac{\theta}{2}\right)\sin\left(\frac{\theta}{2}\right)\cos\left(\frac{3\theta}{2}\right) \tag{1.19}$$

where (r,θ) is the polar coordinate system shown in Fig. 9.

Due to symmetry, only half of the panel is modeled. The nodal arrangement and associated covering used in the *h-p* cloud discretization are depicted in Fig. 10. No special nodal arrangement is used near the singularity at $(0,0)$. Figure 9 shows the finite element mesh used by Szabo [Sza86]. The dimensions of the finite elements decreases in geometric progression towards the singularity. Duarte and Barcellos [DdB91] used a mesh with the same geometric progression but with five layers of elements instead of the three layers as shown in Fig. 9.

The exact strain energy for half of the panel is [Sza86]

$$U\,(u_{x1}^{(1)}, u_{y1}^{(1)}) = 0.23706469 K_I^2 \frac{d}{E}$$

The values $E = K_I = d = 1$ are adopted in the calculations.

In the following, an *h-p* cloud node is said to be *enriched* if the set $\widehat{\mathcal{L}}_p^*$ defined in (1.13) is used to build the *h-p* cloud functions associated with that node. For this

problem the set $\widehat{\mathcal{L}}_p^*$ has always the following elements

$$\widehat{\mathcal{L}}_p^* := \{1, \xi, \eta\} \cup \left\{ u_{xj}^{(1)},\ u_{xj}^{(2)},\ u_{yj}^{(1)},\ u_{yj}^{(2)} \right\}_{j=1,\ldots,p-1}$$

That is, the set $\widehat{\mathcal{L}}_p^*$ has linear polynomials and $p-1$ symmetric and antisymmetric modes from the near crack tip expansion.

Figure 11 shows the convergence in the energy norm of the *h-p* cloud and finite element solutions. There are two curves for the *h-p* cloud method. The solid curve corresponds to the case in which all six nodes shown in Fig. 10 are enriched nodes. The error associated with this discretization is zero for $p \geq 2$ because $\widehat{\mathcal{L}}_{p\geq 2}^*$ contain the exact solution (cf. Theorem 1). The error (of $\mathcal{O}(10^{-6})$ in strain energy) shown in Fig. 11 for $p = 2$ is due to integration errors.

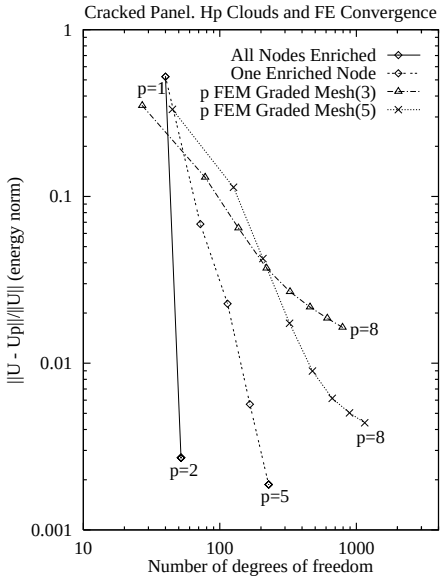

Figure 11 Convergence in the energy norm of the *h-p* cloud and *p* finite element solutions.

This problem was constructed so that the exact solution is equal to the first symmetric mode all over the domain. In practical problems no such restriction applies and the expansion (1.11) (1.12) is valid only in a neighborhood $r < r_0$, $r_0 > 0$ [SB88]. However, far from the crack tip the solution is smooth and can be approximated well by polynomials. Therefore in the general case enriched nodes should be used only in the vicinity of the crack tip. The second curve for the *h-p* cloud method shown in Fig. 11 corresponds to the use of this strategy. More precisely, the curve corresponds to the use of the discretization shown in Fig. 10 with only one enriched node–the one at the crack tip. It can be observed that the *h-p* cloud solution converges at a very high rate, as if the solution was smooth. The convergence of the *p* finite element solution using graded meshes with three (cf. Fig. 9) and five layers of elements is also shown in Fig. 11. It can be observed that the *h-p* cloud discretization requires much fewer

degree of freedoms than the finite element counterpart. An additional advantage of using special functions, made possible by the partition of unity methods framework, is that the stress intensity factors can be obtained, without using elaborate extractions processes, via the approach described in Section 1.3.2.

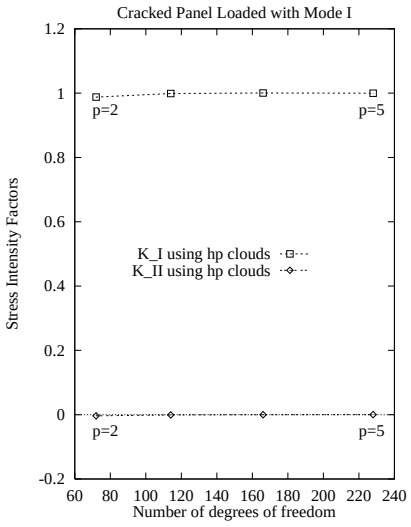

(a) Convergence of the Mode 1 and Mode 2 stress-intensity factors extracted from h-p cloud solutions.

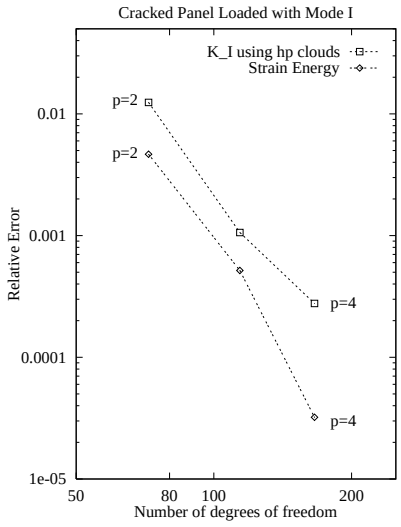

(b) Convergence of the strain energy and the Mode 1 stress-intensity factor extracted from h-p cloud solutions.

Figure 12 Convergence of stress intensity factors.

Figure 12(a) shows the values of K_I and K_{II} obtained using the h-p cloud discretization with only one enriched node and the technique described in Section 1.3.2. The relative errors in strain energy (not energy norm) and the absolute value of the relative error in K_I, computed from the coefficients of the h-p cloud solution, are plotted against the number of degrees of freedom in Fig. 12(b). The stress intensity factor converges at about the same rate as the strain energy and therefore much faster than the error in the energy norm.

Figure 13 shows the computed stress component σ_{22}. The h-p cloud solution corresponds to the discretization with only one enriched node (at $(0,0)$) and $p = 5$. The plot of Fig. 13(a) is in the (θ, r), $0 \leq \theta \leq \pi$, $0.00001 \leq r \leq 1$, plane; θ corresponds to the x direction and r corresponds to the y direction shown in the picture. The effectiveness of the h-p cloud approximation to capture the singularity at $(0,0)$ is evident. Indeed

$$\frac{\text{Max}|\sigma_{22} - \sigma_{22}^{hp}|}{\text{Max}|\sigma_{22}|} = 0.000144$$

where the maximum is taken over all points used to plot Fig. 13(a). Figure 13(b) shows the same results of Fig. 13(a) but this time the plot is done in the (x, y) plane.

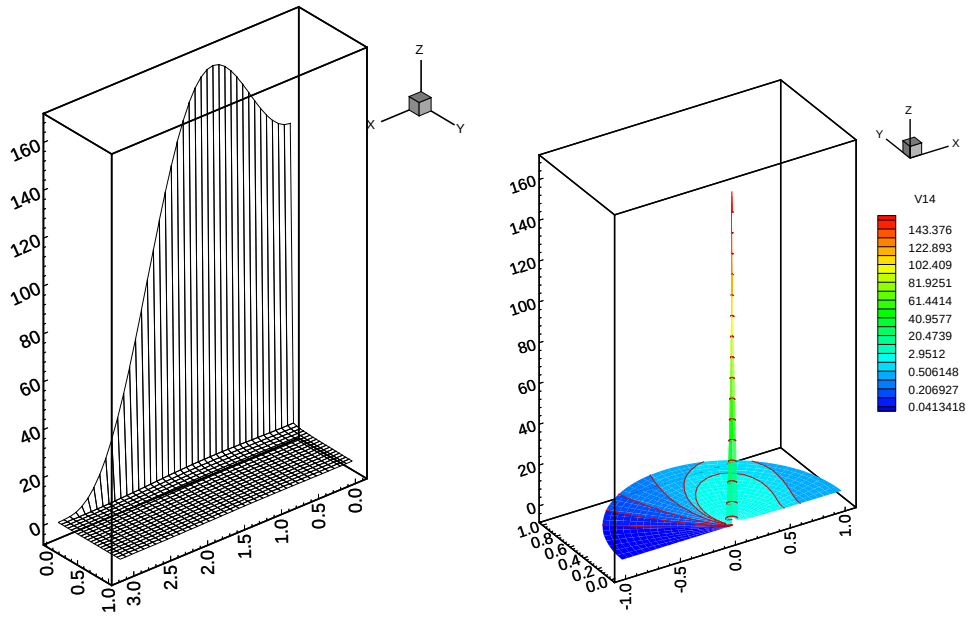

(a) Plot of σ_{22} in the (θ, r) plane.

(b) Plot of σ_{22} in the (x, y) plane.

Figure 13 Stress component σ_{22} computed using h-p clouds.

1.4 CONCLUSIONS

The h-p cloud method is shown to be an extremely effective tool for handling singularities and is particularly effective in computing stress intensity factors in linear elastic fracture mechanics. Experiments suggests the method is exponentially convergent and superior in performance to comparable h-p finite element methods.

Acknowledgment: Preliminary work on this meshless technology was performed under the support of the Army Research Office (J. T. Oden) under contract DAAH04-96-0062. The support of the present work by the National Science Foundation under contract DMI-9561365 and of the CNPq Graduate Fellowship Program (C. A. Duarte) grant # 200498/92-4 is gratefully acknowledged. The authors thank Professor Ivo Babuška from the University of Texas at Austin for fruitful discussion during the course of this investigation.

References

[BKOF96] Belytschko T., Krongauz Y., Organ D., and Fleming M. (1996) Meshless methods: An overview and recent developments. To appear in a Special Issue of *Computer Methods in Applied Mechanics and Engineering* on meshless methods.

[BM95] Babuska I. and Melenk J. M. (July 1995) The partition of unity finite element method. Technical Report BN-1185, Inst. for Phys. Sc. and Tech., University of Maryland.

[DdB91] Duarte C. A. M. and de Barcellos C. S. (December 1991) The element residual method for elasticity and potential problems. In de Las Casas E. B. and de Paula F. A. (eds) *Symposium on Computational Mechanics*, pages 328–335. Belo Horizonte, MG, Brazil. In Portuguese.

[deB78] deBoor C. (1978) *A Practical Guide to Splines*. Springer-Verlag, New York.

[DO] Duarte C. A. M. and Oden J. T.*Hp* clouds—an *hp* meshless method. *Numerical Methods for Partial Differential Equations* (to appear).

[DO95a] Duarte C. A. M. and Oden J. T. (1995) An *hp* adaptive method using clouds. Technical report, TICAM, The University of Texas at Austin. To appear in *Computer Methods in Applied Mechanics and Engineering*.

[DO95b] Duarte C. A. M. and Oden J. T. (1995) Hp clouds–a meshless method to solve boundary-value problems. Technical Report 95-05, TICAM, The University of Texas at Austin.

[Dua95] Duarte C. A. M. (1995) A review of some meshless methods to solve partial differential equations. Technical Report 95-06, TICAM, The University of Texas at Austin.

[LCJ+] Liu W. K., Chen Y., Jun S., Belytschko T., Pan C., Uras R. A., and Chang C. T.Overview and applications of the reproducing kernel particle methods. *Archives of Computational Methods in Engineering. State of Art Reviews* (to appear).

[OB95] Oh H.-S. and Babuska I. (1995) The method of auxiliary mapping for the finite element solutions of elasticity problems containing singularities. *Journal of Computational Physics* 121: 193–212.

[OR76] Oden J. T. and Reddy J. N. (1976) *An Introduction to the Mathematical Theory of Finite Elements*. John Wiley and Sons, New York.

[PB95] Papadakis P. J. and Babuska I. (1995) A numerical procedure for the determination of certain quantities related to the stress intensity factors in two-dimensional elasticity. *Computer Methods in Applied Mechanics and Engineering* 122: 69–92.

[SB88] Szabo B. A. and Babuska I. (1988) Computation of the amplitude of stress singular terms for cracks and reentrant corners. In Cruse T. A. (ed) *Fracture Mechanics: Nineteenth Symposium, ASTM STP 969*, pages 101–124.

[SB91] Szabo B. and Babuska I. (1991) *Finite Element Analysis*. John Wiley and Sons, New York.

[She68] Shepard D. (1968) A two-dimensional function for irregularly spaced data. In *ACM National Conference*, pages 517–524.

[Sza86] Szabo B. A. (1986) Estimation and control of error based on p convergence. In Babuska I., Zienkiewicz O. C., Gago J., and Oliveira E. R. d. A. (eds) *Accuracy Estimates and Adaptive Refinements in Finite Elements Computations*. John Wiley and Sons, New York.